# Component Interactions and Implications for Complex Formation in the Multicomponent Toluene 4-Monooxygenase†

Luke A. Moe, Lea A. McMartin, and Brian G. Fox*

*Department of Biochemistry, College of Agricultural and Life Sciences, University of Wisconsin, Madison, Wisconsin 53706-1544*

*Received January 25, 2006; Revised Manuscript Received March 8, 2006*

ABSTRACT: A fluorophore-labeled form of the T4moD, the catalytic effector protein of the toluene 4-monooxygenase complex, was prepared by engineering the N-terminal region to contain a tetraCys motif and treatment with biarsenical fluorescein. Fluorescence anisotropy was used to study the protein−protein interactions among various combinations of the four components of the complex. Binding interactions were detected between T4moD and the hydroxylase component T4moH [$K_D$ value of 83 nM for interaction with the $\alpha\beta\gamma$ protomer] and between T4moD and the Rieske [2Fe-2S] ferredoxin component T4moC ($K_D$ value of 78 nM). No binding interactions were detected between T4moD and the NADH oxidoreductase component T4moF, but T4moF was able to disrupt binding between T4moC and T4moD. The detected binding interactions suggest an intermediary electron transfer complex between T4moC and T4moD that excludes T4moF. The results indicate that specialization of effector protein function may include specific protein−protein interactions with [2Fe-2S] domains as well as the hydroxylase component.

Toluene 4-monooxygenase (T4MO)[1] is a multicomponent NADH- and $O_2$-dependent enzyme that catalyzes the conversion of toluene to *p*-cresol in the soil bacterium *Pseudomonas mendocina* KR1 (*1*). T4MO is a member of a family of monooxygenases that utilize a diiron cofactor to catalyze the hydroxylation of aliphatic, olefinic, and aromatic hydrocarbons (*2*−*4*). The X-ray structures of MmoH (*5*, *6*) and ToMOH (*7*) revealed the overall conserved features of the hydroxylase component in this enzyme family, including ligands to the catalytically essential diiron center and residues that make up the active sites. On the basis of genetic deductions (*4*) and in accord with functional characterizations, the soluble diiron monooxygenases can be separated into four subfamilies: the soluble methane monooxygenases, the phenol hydroxylases, the $\alpha/\beta$ alkene monooxygenases, and the four-component alkene/aromatic monooxygenases such as T4MO and ToMO. Members of the methane monooxygenase, phenol hydroxylase, and alkene monooxygenase subfamilies are three-protein complexes consisting of an NADH oxidoreductase, an effector protein, and a terminal hydroxylase. In contrast, members of the alkene/aromatic monooxygenase subfamily are four-protein complexes consisting of an NADH oxidoreductase, a Rieske-type ferredoxin, an effector protein, and a terminal hydroxylase.

Figure 1 shows a schematic representation of the four-component T4MO complex. The electron transfer chain portion of the complex consists of T4moF (a 36 kDa FAD- and [2Fe-2S]-containing NADH oxidoreductase) and T4moC (a 12 kDa Rieske-type ferredoxin). T4moC facilitates electron transfer from T4moF to T4moH [a 212 kDa hydroxylase with an $(\alpha\beta\gamma)_2$ quaternary structure and a diiron center present in each α-subunit]. T4moD is an essential 12 kDa cofactorless catalytic effector protein.

Small proteins capable of effecting catalysis have been identified in both heme and non-heme iron monooxygenases (*8*−*10*) and in the diiron desaturases (*11*, *12*). In cytochrome P450cam, putidaredoxin provides both electron transfer and effector functions, including contributions to $O_2$ activation (*13*−*15*). In the diiron monooxygenases, effector proteins have been implicated in myriad effects on catalysis, including enhancing electron transfer between the redox-active components (*9*, *16*), increasing the rate and efficiency of the steady-state reaction (*9*, *16*−*18*), changing the redox potential of the diiron site (*19*), decreasing the activity when present in excess (*20*, *21*), perturbing the spectroscopic features of the diiron site (*20*, *22*, *23*), controlling the rates of reaction with $O_2$ and formation of diiron cofactor intermediates (*24*), acting as a gating component for $O_2$ access and substrate (*25*), altering substrate selectivity and the regiospecificity of hydroxylation (*18*, *26*), and promoting a global conformation change of the hydroxylase dimer (*27*). In addition,

† This work was supported by the National Science Foundation (Grant MCB-0316232 to B.G.F.).

* To whom correspondence should be addressed: phone, (608) 262-9708; fax, (608) 262-3453; e-mail, bgfox@biochem.wisc.edu.

[1] Abbreviations: T4MO, four-protein toluene 4-monooxygenase complex from *Pseudomonas mendocina* KR1; T4moH, hydroxylase component of T4MO; T4moC, Rieske-type [2Fe-2S] component of T4MO; T4moD, catalytic effector protein component of T4MO; T4moF, NADH oxidoreductase component of T4MO; FlAsH, biarsenical fluorescein-derived fluorophore; C4-T4moD, a T4moD construct with an N-terminal tetraCys motif; f-T4moD, C4-T4moD labeled with FlAsH; ΔN4-T4moD, a T4moD construct having four amino acids deleted from the N-terminus; MMO, soluble methane monooxygenase; MmoB, effector protein of MMO; MmoH, hydroxylase component of MMO; MmoR, reductase component of MMO; TbuB, Rieske-type ferredoxin of the toluene monooxygenase from *Ralstonia pickettii* PK01; BphF, Rieske-type ferredoxin of the biphenyl dioxygenase from *Burkholderia* sp. strain LB400; TCEP, tris(2-carboxyethyl)phosphine hydrochloride; ToMO, toluene/*o*-xylene monooxygenase from *Pseudomonas stutzeri* OX1; ToMOH, hydroxylase component of ToMO.

10.1021/bi0601611 CCC: $33.50 
Published on Web 04/06/2006

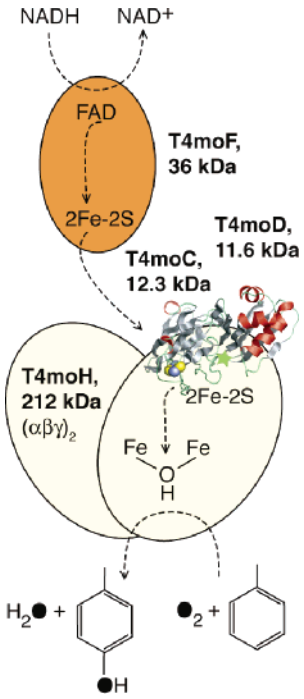


FIGURE 1: Schematic representation of the T4MO complex: T4moF, 36 kDa NADH oxidoreductase component; T4moC, 12 kDa Rieske-type ferredoxin; T4moD, 12 kDa effector protein; T4moH, 212 kDa $(\alpha\beta\gamma)_2$ diiron hydroxylase component. Cofactors in each component are indicated; the dashed arrows represent electron flow within the T4MO complex. The $O_2$-dependent conversion of toluene to *p*-cresol occurs at the diiron center in T4moH.

studies of MMO have indicated that binding of MmoR to MmoH changes the redox potential of the diiron site (*19*, *28*) and the rate of decay of diiron intermediates (*28*) and alters product yield (*28*, *29*). The soluble diiron enzymes also undergo autoxidation reactions and uncoupling of electron transfer when assembled as a nonoptimal complex or when presented with difficult to oxidize nonnatural substrates (*18*, *20*, *29*). Thus protein interactions provide essential contributions needed to generate a powerful oxidizing species and direct it to efficiently carry out chemically difficult oxidation reactions.

The existence of four-component diiron hydroxylase complexes such as T4MO introduces questions regarding the nature of component interactions beyond those inherent in the three-component hydroxylases such as MMO. Here we have used fluorophore-labeled T4moD and fluorescence anisotropy measurements to study the binding interactions among the four protein components of T4MO. The results provide new insight into the molecular interactions involved in multiprotein catalysis and the potential origins of specificity for protein interactions required by T4MO. The implications of these results for complex formation during steady-state catalysis and the potential for formation of inhibitory complexes are discussed.

## MATERIALS AND METHODS

*Materials.* Enzyme substrates, products, reagents for synthesis of FlAsH-$EDT_2$, and other chemicals, as well as lysozyme, DNase, and RNase, were from Sigma-Aldrich (St. Louis, MO). Gateway reagents, FlAsH standard, and the plasmids pDONR221 and pDEST17 were from Invitrogen

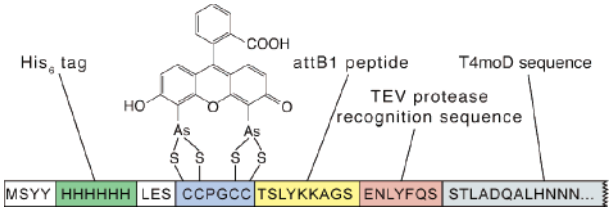


FIGURE 2: Schematic representation of the engineered primary sequence at the N-terminus of fluorescently labeled T4moD. The $His_6$ tag allows purification by $Ni^{2+}$-immobilized metal affinity chromatography. The biarsenical fluorescein derivative (FlAsH) is shown bound to the tetraCys motif. The attB1 peptide (TSLYKKAGS) and the tobacco etch virus (TEV) protease recognition sequence arise from Gateway cloning and potential need to remove the N-terminal tag. For this work, the N-terminal tag was not removed. The Met1 codon was eliminated from the *tmod* gene during the PCR cloning, and only the first 12 N-terminal amino acids of T4moD are indicated to conserve space.

(Carlsbad, CA). The plasmid pVP14 was created previously (*30*). PCR primers were from Integrated DNA Technologies, Inc. (Coralville, IA). Yield Ace DNA polymerase was from Stratagene (La Jolla, CA). DNA purification kits were from Qiagen (Valencia, CA). Competent *Escherichia coli* strains Top 10 (Invitrogen) and BL21(DE3) (Novagen, Madison, WI) were used for cloning and expression, respectively. Big Dye terminator version 3.1 mix (Applied Biosystems, Foster City, CA) was used for DNA sequencing at the University of Wisconsin—Madison Biotechnology Center. Cell growth and protein purification reagents were from Fisher (Fair Lawn, NJ). TCEP was from Pierce (Rockford, IL).

*Preparation of Expression Plasmids.* A two-step PCR protocol (*31*) was used to amplify the *tmod* gene from pRS184f (*32*) with flanking 5′ and 3′ sequences encoding the tobacco etch virus protease recognition sequence and *attB1* recombination sites. The first step PCR primers were T4DentryF (5′-AACCTGTACTTCCAGTCCAGCACATTGGCTGATCAGGCTTTAC-3′) and T4DentryR (5′-GTACAAGAAAGCTGGGTCCTACATGGTTTTATCAAAGTAGAAGCG-3′). Universal primers for the second step of the PCR reaction are reported elsewhere (*31*). The PCR product of the two-step amplification was transferred into pDONR221 by BP recombination to form the entry plasmid pLAM01. The entry plasmid was sequenced using M13F primers to verify the amplified DNA sequence. The expression vector pLAM02 was created by LR recombination between pLAM01 and pVP14. The BP and LR recombination steps were done according to the manufacturers' protocols. Figure 2 shows a schematic representation of the protein product generated by expression from pLAM02.

*Synthesis of the FlAsH Fluorophore.* FlAsH was prepared from fluorescein mercuric acetate (*33*, *34*). The reaction progress was monitored on silica gel thin-layer chromatography plates in 25% ethyl acetate, 70% toluene, and 5% acetic acid by comparison to a commercial FlAsH standard. To obtain the product as the ethanedithiol adduct, the initial reaction mixture was added to 50 mL of a 1:1 mixture of 2 M MOPS with acetone containing 0.5 mL of ethanedithiol. Chloroform (30 mL) was then added to the mixture, and acetic acid was added until the color of the solution stopped changing. This mixture was stirred for 1 h. The aqueous layer was extracted twice with 20 mL of chloroform, and the resultant solution was dried overnight with anhydrous magnesium sulfate. The mixture was decanted, and the

chloroform was evaporated under a stream of argon. The dry product was dissolved into 100 $\mu$L of chloroform and further purified by silica column chromatography (*35*). Fractions of the purified product were identified on the basis of the visual intensity of pink color. The solvent was removed from each of the identified fractions, and the product was redissolved in 100 $\mu$L of DMSO.

The relative fluorescence of each fraction was then determined by comparison of the fluorescence intensity of the FlAsH fluorophore bound to purified maltose binding protein engineered to contain a C-terminal tetraCys motif (*30*) versus the fluorophore in buffer alone. This was accomplished by dilution of 1 $\mu$L of the fractions dissolved in DMSO by 1:500 into 20 mM sodium phosphate, pH 7.5, containing 100 mM NaCl and 0.3 mM TCEP. Further 5× serial dilutions were occasionally necessary, depending on the concentration of the FlAsH preparation. The diluted fractions were then mixed with a 5 $\mu$M solution of the tetraCys-engineered maltose binding protein or buffer. The fluorescence (500 nm excitation; 535 nm emission) was measured as a function of time using a SpectraMAX Gemini XS plate reader (Molecular Devices, Sunnyvale, CA). When the maximum fluorescence was obtained, fractions that gave at least 100-fold greater fluorescence with tetraCys-engineered maltose binding protein as compared to unbound fluorophore were retained and further analyzed by electrospray mass spectroscopy in negative ion mode at the University of Wisconsin—Madison Biotechnology Center. The most highly purified samples exhibited a −1 charge molecular ion of 663 Da. Fractions meeting the fluorescence intensity threshold and the mass spectral assignment were considered to be pure and were pooled. The concentration of the pooled fluorophore preparation was determined using $\epsilon_{507} = 4.1\times 10^4\ M^{-1}\ cm^{-1}$ (*34*).

*Protein Expression.* Expression and purification of the other T4MO proteins were as previously described (*21*, *32*), except that a revised protocol for expression and purification of T4moF will be reported elsewhere. The C4-T4moD was expressed using the same methods as for T4moD (*21*). TbuB was purified using the same protocol as used for T4moC (*36*).

C4-T4moD was purified from a frozen bacterial cell pellet, typically 5−10 g of wet cell paste, resuspended in an equal volume (w/v) of 20 mM $NaH_2PO_4$, pH 7.5, containing 500 mM NaCl and 0.3 mM TCEP (buffer A). Lysozyme, DNase, and RNase (0.5 mg each) were also added to the resuspension buffer. The resuspended cells were sonicated (Fisher Model 550 sonic dismembrator at 50% maximum) in a stainless steel beaker at 4 °C for ∼4 min total using 10 s pulses. The sonicated cells were centrifuged at 19000 rpm for 45 min. The supernatant was decanted and diluted with an equal volume of buffer A. The diluted supernatant was immediately loaded onto a HisTrap column (Amersham Biosciences, Piscataway, NJ) preconditioned in buffer A with 0.2 M $NiSO_4$ attached to an AKTA FPLC system (Amersham Biosciences). The column was washed with two volumes of buffer A with 50 mM imidazole and then eluted by a linear gradient from 50 to 500 mM imidazole in buffer A over 15 column volumes. Fractions containing C4-T4moD were identified by SDS−PAGE using a sample loading buffer containing FlAsH-$EDT_2$ (10 $\mu$M), followed by fluorescence imaging of the gel using a Typhoon 9410 variable mode imager (Amersham Biosciences) (488 nm excitation; 520 nm emission). The FlAsH detection results were corroborated by traditional Coomassie staining. The purified protein was concentrated by ultrafiltration (Amicon, Beverly MA) and exchanged into 20 mM $NaH_2PO_4$ buffer, pH 7.5, containing 100 mM NaCl and 0.3 mM TCEP using Sephadex G-50 (Amersham Biosciences).

*Fluorophore Labeling.* Purified C4-T4moD (∼11 mg) was labeled with FlAsH by addition of a 10−20% molar excess of FlAsH-$EDT_2$. The labeling reaction was determined to be complete after ∼5 h by monitoring the increase in fluorescence intensity (488 nm excitation; 535 nm emission) but typically allowed to continue overnight at room temperature for convenience. The labeled protein sample was cleaned up by gel filtration using a Sephacryl 26/60 S100 fast-flow column (Amersham Biosciences) at a linear flow rate of 10 cm/h. This step eliminated the excess FlAsH-$EDT_2$ reagent and separated the labeled monomeric f-T4moD from other multimeric T4moD aggregates. Aliquots of the concentrated f-T4moD (∼2 mg total recovered) were drop frozen in liquid $N_2$ and stored at −80 °C until use.

*Fluorescence Anisotropy Measurements.* All binding studies were performed on concentrated protein stocks diluted into 50 mM phosphate buffer, pH 7.5, containing 2% glycerol and 50 mM NaCl. Protein concentrations of f-T4moD were determined using the Bio-Rad protein assay dye reagent (Bio-Rad, Hercules, CA) with bovine serum albumin (Pierce) as the standard. The concentration of T4moH reported is that of the $\alpha\beta\gamma$ protomer. The binding measurements were performed in Greiner 384-well flat-bottom plates (Greiner Bio-One, Longwood, FL) in a total sample volume of 100 $\mu$L. All measurements were taken in quadruplicate at room temperature. Fluorescence anisotropy was measured as $r = (f_\perp - f_\parallel)/(f_\perp + 2f_\parallel)$, where $f_\perp$ is the fluorescence intensity measured perpendicular to the excitation direction and $f_\parallel$ is the fluorescence intensity measured parallel to the excitation and reported as millianisotropy, $mr = 0.001r$. Measurements were taken on a Tecan Ultra384 spectrofluorometer (Tecan, Zurich, Switzerland) using a 485 nm excitation (25 nm band-pass). Fluorescence emission was detected at 535 nm (20 nm band-pass) with a 40 $\mu$s integration time. The $g$ value for all experiments was 1.1007.

*Binding Analysis.* Changes in anisotropy values were calculated as $\Delta r = r - r_{min}$, where $r$ is the observed anisotropy and $r_{min}$ is the minimum anisotropy value. Anisotropy values were converted to a fraction of the fluorescent species bound as $f_b = \Delta r/[r_{max} - r_{min}]$, where $r_{max}$ is the maximum anisotropy value measured and the other variables were as previously defined. Least-squares regressions of the experimental anisotropy data were done with fraction bound as the target function using SigmaPlot 9.0 (Systat Software Inc., Point Richmond, CA).

*Catalytic Assays.* Reconstitution of the T4MO complex and determination of catalytic activity were as previously described (*18*).

## RESULTS

*Preparation and Function of f-T4moD.* The cloning strategy utilized here was originally designed to incorporate a tobacco etch virus protease cleavable N-terminal sequence (∼4 kDa) containing a $His_6$ tag and FlAsH-binding motif

onto genomic open reading frames (*30*). Figure 2 shows a schematic of the N-terminal region of the protein expressed from pLAM02. The C4-T4moD could be purified from a cell lysate in a single step by $Ni^{2+}$-immobilized metal affinity chromatography. For the studies reported here, the N-terminal tag was retained in order to allow fluorescence labeling. After an overnight labeling reaction and cleanup by gel filtration chromatography, a purified sample of f-T4moD was obtained. When examined in side-by-side reactions for reconstitution of toluene hydroxylation by the four-protein T4MO complex, native T4moD, C4-T4moD, and f-T4moD gave catalytic parameters that were not distinguishable within experimental error from previous results (*37*). This finding is in accord with previous studies demonstrating that removal of the N-terminus from T4moD also had little impact on the catalytic properties (*37*).

*Fluorescence Anisotropy of f-T4moD.* Preliminary studies of f-T4moD in the absence of a binding partner showed protein concentration-dependent decreases in anisotropy and fluorescence intensity upon dilution of the concentrated protein preparation into the buffer used for the binding studies. This behavior is consistent with a slow relaxation of the concentrated protein from an aggregated state to a monomeric preparation upon dilution. Therefore, all binding measurements were obtained using 5 nM f-T4moD after an incubation period of 20−40 min. During titrations of f-T4moD with the other proteins, the total fluorescence intensity remained constant within ~10%, suggesting that the fluorophore remained in the same chemical environment upon complex formation.

*Titration of f-T4moD with T4MO Components.* Figure 3A shows a plot of the fraction bound obtained from titration of T4moH into a fixed concentration of f-T4moD. The least-squares analysis suggested a single site binding between f-T4moD and the $\alpha\beta\gamma$ protomer of T4moH with a $K_D$ value of 83 ± 5 nM. Figure 3B shows a plot of the fraction bound from titration of T4moC into a fixed concentration of f-T4moD. In this case, the least-squares analysis again suggested a single site-binding interaction between f-T4moD and T4moC, but with a $K_D$ value of 78 ± 7 nM.

The soluble portions of the Rieske protein from *Thermus thermophilus* (*38*), the Rieske-type ferredoxin of the biphenyl dioxygenase from *Burkholderia* sp. strain LB400 (BphF) (*39*), and the Rieske-type ferredoxin of the toluene monooxygenase from *Ralstonia pickettii* (TbuB) (*40*) were also examined for binding interactions with f-T4moD. Of these, only TbuB showed a significant interaction with f-T4moD, and Figure 3C shows the plot of fraction bound versus TbuB concentration. Least-squares fitting yielded a $K_D$ value for TbuB (550 ± 70 nM) that was ~7× greater than that measured with T4moC (78 nM).

Figure 4 shows a semilogarithmic plot of the results obtained from titration of f-T4moD with T4moH along with results obtained in the presence of two different concentrations of T4moC. In the presence of less than 1 nM T4moH, f-T4moD had m*r* ≈ 100, while the complexes of f-T4moD fully bound either with T4moH or with T4moC had m*r* ≈ 210 (see Figure 4). The overall similarity of the maximum m*r* values observed for these three complexes arises from the interrelationship between excited state lifetime [~3 ns for fluorescein (*41*)] and the rotational correlation times of proteins [~10 ns for a 25 kDa protein (*42*)]. Consequently,

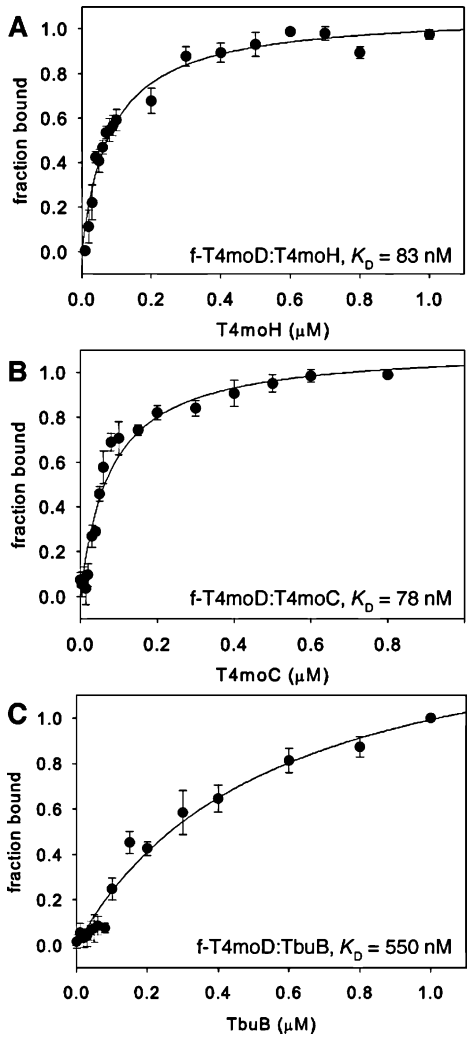


FIGURE 3: Fraction bound plots showing the binding interactions with f-T4moD as detected by fluorescence anisotropy. f-T4moD was present at a fixed concentration of 5 nM in all experiments, and the other proteins were added during titrations. $K_D$ values were determined by nonlinear regression using a single-site binding model, and best-fit lines are shown as the solid line in each plot. (A) T4moH, $K_D$ = 83 nM. (B) T4moC, $K_D$ = 78 nM. (C) TbuB, $K_D$ = 550 nM.

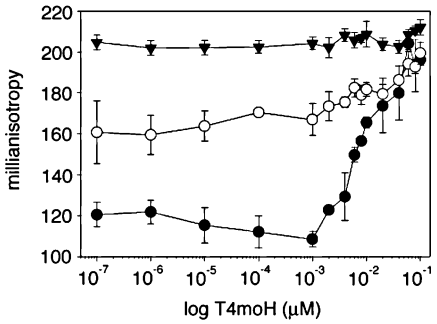


FIGURE 4: Semilogarithmic plot of the change in anisotropy detected during the titration of f-T4moD with T4moH in the presence of increasing amounts of T4moC. f-T4moD was present at a fixed concentration of 5 nM in all experiments. T4moH was added by titration, and T4moC was present at the following fixed concentrations: no T4moC present (solid circles); 100 nM T4moC (open circles); 1 μM T4moC (filled triangles).

the fluorescence anisotropy of fluorescein derivatives attached to proteins is only sensitive to changes in mass up to ~30 kDa, while formation of larger complexes gives only

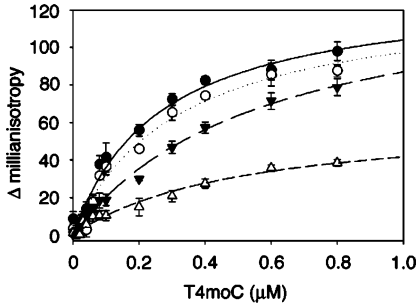


FIGURE 5: Plot of the change in anisotropy of f-T4moD upon titration with T4moC in the presence of different, fixed concentrations of T4moF. f-T4moD was present at a fixed concentration of 5 nM in all experiments. T4moC was added by titration, and T4moF was present at the following fixed concentrations: none (solid circle); 10 nM (open circle); 100 nM (filled triangle); 1 $\mu$M (open triangle). Measurements performed with 500 nM T4moF reproduced the results obtained with 1 $\mu$M T4moF and are not shown.

limited further increases in anisotropy. This experimental limitation precludes the conclusive identification of a ternary complex of f-T4moD, T4moC, and T4moH by this approach.

*Binding of T4moF and f-T4moD to T4moC.* Titration of T4moF into a fixed concentration of f-T4moD gave no significant change in the anisotropy up to a T4moF concentration of 2 $\mu$M (data not shown), indicating that a complex is not formed between these two components. Since T4moF and T4moC must interact with each other during electron transfer (Figure 1), the binding interactions detected between T4moC and T4moD introduced the question of whether the presence of T4moF might influence the formation of this complex. Figure 5 shows results from a series of binding studies where a fixed concentration of f-T4moD was titrated with changing concentrations of T4moC in the presence of fixed, increasing concentrations of T4moF. The results show that the binding affinity between T4moC and T4moD decreased as the concentration of T4moF was increased. In these experiments, a ~3-fold increase in the $K_D$ for the interaction of f-T4moD and T4moC was observed at the maximum concentration of T4moF investigated.

*Titration of f-T4moD with T4moD.* Previous catalytic and structural studies have indicated the potential for dimerization of effector proteins (*20*, *43*). To further investigate this interaction in the T4MO complex, fixed concentrations of f-T4moD were titrated with native T4moD and with ΔN4-T4moD, a variant with four amino acids removed from the N-terminus. The X-ray crystal structures of these latter forms of T4moD are known (*37*), and other than changes in the N-terminal region, they are structurally indistinguishable and have comparable catalytic properties. Figure 6 shows semilogarithmic plots produced from these titration results. Both T4moD isoforms gave saturation-binding curves with f-T4moD. A $K_D$ value of 2.4 ± 0.3 $\mu$M was determined for reaction with T4moD, and a $K_D$ value of 790 ± 100 nM was determined for reaction with ΔN4-T4moD. The difference in these $K_D$ values suggests that the presence of the N-terminus can weaken self-dimerization interactions of T4moD. Figure 6 also shows that as the ΔN4-T4moD concentration approached ~10 $\mu$M, the observed anisotropy decreased. This may correspond to release of f-T4moD from the heterologous complex, as self-dimerization of ΔN4-T4moD would be favored at higher concentrations and thus release the f-T4moD.

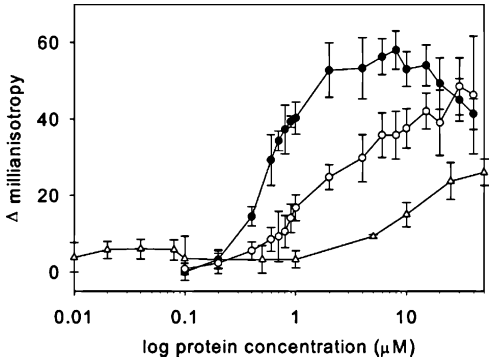


FIGURE 6: Semilogarithmic plot of the change in anisotropy detected during the titration of f-T4moD with T4moD, ΔN4-T4moD, and lysozyme. f-T4moD was present at a fixed concentration of 5 nM in all experiments. The following other proteins were added during titrations: native T4moD (open circles); ΔN4-T4moD (closed circles); lysozyme (open triangles). f-T4moD (p$I$ = 4.99) and lysozyme (p$I$ = 11.35) are acidic and basic proteins, respectively, and would be predicted to have weak electrostatic interactions.

Control experiments were conducted to investigate the possibility of nonspecific protein−protein interactions under the experimental conditions utilized. Thus f-T4moD (15.6 kDa, p$I$ = 4.99) was titrated with lysozyme [14.3 kDa, p$I$ = 11.35 (*44*, *45*)]. Figure 6 indicates weak, nonspecific binding between f-T4moD and lysozyme at concentrations above ~5 $\mu$M.

## DISCUSSION

The role of component interactions in catalysis has been studied in other multicomponent oxygenases and electron transfer complexes (*15*, *46*−*48*), including the three-component diiron hydroxylases best represented by MMO and most relevant to the present studies (*9*, *20*, *29*). These interactions provide physical control of reactivity and profoundly influence the outcome of stereo- and regiospecific reactions. The present results provide new details regarding component interactions in T4MO, a four-component diiron monooxygenase.

*Dimerization of Effector Proteins.* The effector proteins range in size from ~10 to 17 kDa, with the variability primarily in the N-terminal region (*21*). The MmoB effector protein of soluble MMO has ~33 disordered residues at the N-terminus, while effector proteins of the aromatic/alkene monooxygenase subfamily such as T4moD have ~13 residues, and effector proteins of the phenol hydroxylase subfamily have ~3 residues. There is no primary sequence conservation in the N-terminal region across these catalytic subclasses, and functional consequences of altering the N-terminus are also varied. Thus deletion of the N-terminus from MmoB resulted in a complete loss of steady-state activity without preventing binding to MmoH (*43*, *49*, *50*). In contrast, removal of up to 10 residues from the N-terminus of T4moD had no significant consequences on either catalysis ($k_{cat}$, apparent $K_M$, $K_I$, coupling, regiospecificity of aromatic hydroxylation) or the structure of the remaining, well-folded portion of the protein (*37*).

In vitro, T4moD and ΔN4-T4moD can act as inhibitors of the catalytic reaction, with $K_I$ values on the order of ~100 $\mu$M (*37*). There is evidence, including results presented here, that effector proteins can undergo dimerization (*20*, *43*). The

results of Figure 6 indicate that removing four residues from the N-terminus of T4moD gave a 3-fold tighter binding in the dimerization with f-T4moD ($K_D$ = 790 nM) as compared to dimerization with native T4moD ($K_D$ = 2.4 $\mu$M), suggesting that the presence of the complete N-terminus of T4moD may help to minimize this inhibitory protein−protein interaction. These $K_D$ values for dimerization are ~10−30× larger than the $K_D$ values for the binary interactions detected between f-T4moD and either T4moC or T4moH. In certain circumstances, a higher order oligomerization of T4moD may also be occurring. Indeed, examination of the extended molecular interactions in the T4moD crystals (PDB accession numbers 2BF2, 2BF3, and 2BF5)[2] showed a pairing of $\beta$-strand edges reminiscent of amyloid formation.

*Catalytic Complexes Formed in T4MO*. Tight binding interactions were detected between T4moC and T4moD and between T4moD and T4moH. It is noted that T4moC (12.3 kDa, p$I$ = 4.26) and f-T4moD (15.6 kDa, p$I$ = 4.99) have predicted repelling charge states at the pH of the binding study, yet have a high-affinity binding interaction. This affinity suggests that specific complementarily charged surfaces might be used for the interaction. For comparison, a weaker binding interaction was observed between T4moD and TbuB, a Rieske-type ferredoxin closely related to T4moC, while no binding interactions were observed with the more distantly related *Thermus* and BphF Rieske proteins. Furthermore, binding studies with lysozyme provided a control for nonspecific interactions, which were indeed observed, but at >100-fold higher protein concentrations than those needed for the specific interactions of T4moD with either T4moC or T4moH. The nonspecific interactions between f-T4moD and lysozyme likely derive from the attracting charge states of these two proteins at the pH of the binding study (*51*). This interaction has an affinity comparable to the self-association interaction described above for T4moD, which is, again, ~100× weaker than the specific interactions detected between T4moD and the other protein components of the T4MO complex.

In principle, a series of binary interactions between protein pairs might be sufficient to support catalysis in the T4MO complex. By consideration of electron transfer events alone, a minimal model for T4MO component interactions would include binding events between T4moF and T4moC and then separate interactions between T4moC and T4moH. For example, NADH-reduced T4moF and oxidized T4moC could interact independently to yield reduced T4moC, and then reduced T4moC could interact with oxidized T4moH. However, this simple model does not account for the experimental evidence (Figure 3) that a high concentration of T4moF can interfere with the binding of T4moC and T4moD (Figure 5) and that T4moD has binding interactions of similar affinity with both T4moC (apparent $K_D$ = 83 nM) and T4moH (apparent $K_D$ = 78 nM). Likewise, it does not consider the kinetic sequence for binding of either T4moC or T4moD to T4moH and whether the T4moC−T4moD complex might also bind to T4moH.

*Interactions of T4moC, T4moD, and T4moF*. Both MmoR and T4moF have a three-domain configuration, with a similar sequential arrangement of [2Fe-2S], flavin, and NADH binding subdomains. It is therefore intriguing that binding interactions between MmoB and MmoR have been previously detected (*20*, *28*), while no interactions were detected between T4moD and T4moF. One possible way to reconcile this apparent difference between the three- and four-component complexes would be to consider that effector protein binding might be, in part, directed toward a [2Fe-2S] domain of the electron transfer components. Since the three-dimensional structures and other biophysical properties of the Rieske and plant-type ferredoxins are distinct, T4moD may have a unique affinity for the Rieske-type [2Fe-2S] fold, while MmoB would have affinity for the plant-type [2Fe-2S] fold. These different affinities would be consistent with the patterns of cross-reactivity established for the effector proteins, as an effector protein from the aromatic/alkene monooxygenase subfamily (which use an intermediate Rieske ferredoxin) partially substituted for T4moD, but effector proteins from the phenol hydroxylase subfamily (*21*) and MmoB from *Methylosinus trichosporium* OB3b (*18*) did not (and do not use an intermediate Rieske ferredoxin). This difference conceivably arises from changes in the surfaces of the otherwise homologous structures of the effector proteins (*37*) and the different structures of the ferredoxin domains [e.g., PDB accession numbers 1vm9 and 1jq4 (*52*)].

While T4moD apparently does not bind to T4moF, Figure 5 indicates that T4moF is capable of interfering with the interactions between T4moC and T4moD. This could arise by the existence of overlapping binding sites on T4moC for these two other components or by an allosteric change in T4moC caused by T4moF binding that decreased the affinity for T4moD. This latter scenario seems unlikely given that T4moC has a well-defined, compact structure (PDB accession number 1vm9), and significant changes in protein backbone are not anticipated upon oxidation/reduction cycling of ferredoxins (*53*, *54*).

*Nature of the T4MO Catalytic Complex.* A ternary complex has been implicated in the MMO complex (*20*, *26*, *28*, *29*). It is reasonable that the four-component hydroxylases might also form a ternary protein complex during catalysis. The similar binding affinities for the binary complexes of T4moD with both T4moC and T4moH detected here suggest that a ternary complex might also form from these components during catalysis. Thus the four-component hydroxylases might substitute T4moC for MmoR. By first formation of a binary complex between T4moC and T4moD, the binding surface available for interaction with T4moH might be increased or become uniquely shaped or charged, leading to specificity for binding to T4moH in a ternary complex that is not available from binary interactions.

Intuitively, the MMO ternary complex would seem to be more effective for electron transfer than the proposed ternary assembly from the four-component monooxygenases, as MmoR (containing both FAD and [2Fe-2S]) can react with NADH and potentially provide both of the reducing equivalents required for the monooxygenase reaction from a single complex, whereas T4moC cannot, as it is only a $1e^-$ carrier. Nevertheless, there are a number of examples where $1e^-$ carriers efficiently participate in $2e^-$ reactions. Significant details have emerged for how cytochrome P450 regulates catalysis via $1e^-$ steps (*15*, *55*). It is not clear at present how the stoichiometry and timing of protein binding and electron transfer are efficiently achieved in the four-component diiron

[2] G. Lountos, B. G. Fox, and A. M. Orville, unpublished results.

complexes such as T4MO or in other diiron enzymes such as stearoyl-ACP desaturase, where the obligate $1e^-$ donor is a plant-type [2Fe-2S] ferredoxin (*11*), or in alkane hydroxylase, where the $1e^-$ donor is a rubredoxin (*56*). These studies provide new insight into the potential pairwise interactions of the four-component hydroxylases. Further elucidation of the properties of these protein complexes may shed light on this interesting problem of biological specificity and energy coupling.

## ACKNOWLEDGMENT

The authors thank Dr. James A. Fee (The Scripps Research Institute) and Prof. Lindsay Eltis (University of British Columbia) for generous gifts of purified *T. thermophilus* Rieske protein and BphF used in this work.

## REFERENCES

1. Whited, G. M., and Gibson, D. T. (1991) Toluene-4-monooxygenase, a three component enzyme system that catalyzes the oxidation of toluene to *p*-cresol in *Pseudomonas mendocina* KR1, *J. Bacteriol. 173*, 3010−3016.
2. Wallar, B. J., and Lipscomb, J. D. (1996) Dioxygen activation by enzymes containing binuclear non-heme iron clusters, *Chem. Rev. 96*, 2625−2657.
3. Fox, B. G. (1998) in *Comprehensive Biological Catalysis* (Sinnott, M., Ed.) pp 261−348, Academic Press, London.
4. Leahy, J. G., Batchelor, P. J., and Morcomb, S. M. (2003) Evolution of the soluble diiron monooxygenases, *FEMS Microbiol. Rev. 27*, 449−479.
5. Rosenzweig, A. C., Frederick, C. A., Lippard, S. J., and Nordlund, P. (1993) Crystal structure of a bacterial non-haem iron hydroxylase that catalyses the biological oxidation of methane, *Nature 336*, 537−543.
6. Elango, N., Radhakrishnan, R., Froland, W. A., Wallar, B. J., Earhart, C. A., Lipscomb, J. D., and Ohlendorf, D. H. (1997) Crystal structure of the hydroxylase component of methane monooxygenase from *Methylosinus trichosporium* OB3b, *Protein Sci. 6*, 556−568.
7. Sazinsky, M. H., Bard, J., Di Donato, A., and Lippard, S. J. (2004) Crystal structure of the toluene/*o*-xylene monooxygenase hydroxylase from *Pseudomonas stutzeri* OX1, *J. Biol. Chem. 279*, 30600−30610.
8. Sligar, S. G., Debrunner, P. G., Lipscomb, J. D., Namtvedt, M. J., and Gunsalus, I. C. (1974) A role of the putidaredoxin COOH-terminus in *P*-$450_{cam}$, *Proc. Natl. Acad. Sci. U.S.A. 71*, 3906−3910.
9. Green, J., and Dalton, H. (1985) Protein B of soluble methane monooxygenase from *Methylococcus capsulatus* (Bath), *J. Biol. Chem. 260*, 15795−15801.
10. Brazeau, B. J., Wallar, B. J., and Lipscomb, J. D. (2003) Effector proteins form P450cam and methane monooxygenase: lessons in tuning nature's powerful reagents, *Biochem. Biophys. Res. Commun. 312*, 143−148.
11. Lyle, K. S., Haas, J. A., and Fox, B. G. (2003) Rapid-mix and chemical quench studies of ferredoxin-reduced stearoyl-acyl carrier protein desaturase, *Biochemistry 42*, 5857−5866.
12. Fox, B. G., Lyle, K. S., and Rogge, C. E. (2004) Reactions of the diiron enzyme stearoyl-ACP desaturase, *Acc. Chem. Res. 37*, 421−429.
13. Lipscomb, J. D., Sligar, S. G., Namtvedt, M. J., and Gunsalus, I. C. (1976) Autooxidation and hydroxylation reactions of oxygenated cytochrome P-$450_{cam}$, *J. Biol. Chem. 251*, 1116−1124.
14. Shimada, H., Nagano, S., Hori, H., and Ishimura, Y. (2001) Putidaredoxin-cytochrome P450cam interaction, *J. Inorg. Biochem. 83*, 255−260.
15. Denisov, I. G., Makris, T. M., Sligar, S. G., and Schlichting, I. (2005) Structure and chemistry of cytochrome P450, *Chem. Rev. 105*, 2253−2277.
16. Fox, B. G., Froland, W. A., Dege, J. E., and Lipscomb, J. D. (1989) Methane monooxygenase from *Methylosinus trichosporium* OB3b: Purification and properties of a three-component system with high specific activity from a type II methanotroph, *J. Biol. Chem. 264*, 10023−10033.
17. Pikus, J. D., Studts, J. M., Achim, C., Kauffmann, K. E., Münck, E., Steffan, R. J., McClay, K., and Fox, B. G. (1996) Recombinant toluene 4-monooxygenase: Catalytic and Mössbauer studies of the purified diiron and Rieske components of a four-protein complex, *Biochemistry 35*, 9106−9119.
18. Mitchell, K. H., Studts, J. M., and Fox, B. G. (2002) Combined participation of effector protein binding and hydroxylase active site residues provide toluene 4-monooxygenase regiospecificity, *Biochemistry 41*, 3176−3188.
19. Paulsen, K. E., Liu, Y., Fox, B. G., Lipscomb, J. D., Münck, E., and Stankovich, M. T. (1994) Oxidation−reduction potentials of the methane monooxygenase hydroxylase component from *Methylosinus trichosporium* OB3b, *Biochemistry 33*, 713−722.
20. Fox, B. G., Liu, Y., Dege, J. E., and Lipscomb, J. D. (1991) Complex formation between the protein components of methane monooxygenase from *Methylosinus trichosporium* OB3b: Identification of the sites of component interactions, *J. Biol. Chem. 266*, 540−550.
21. Hemmi, H., Studts, J. M., Chae, Y. K., Song, J., Markley, J. L., and Fox, B. G. (2001) Solution structure of the toluene 4-monooxygenase effector protein (T4moD), *Biochemistry 40*, 3512−3524.
22. Fox, B. G., Hendrich, M. P., Surerus, K. K., Andersson, K. K., Froland, W. A., Lipscomb, J. D., and Münck, E. (1993) Mössbauer, EPR and ENDOR studies of the hydroxylase and reductase components of methane monooxygenase from *Methylosinus trichosporium* OB3b, *J. Am. Chem.* Soc. *115*, 3688−3701.
23. Hendrich, M. P., Münck, E., Fox, B. G., and Lipscomb, J. D. (1990) Integer-spin EPR studies of the fully reduced methane monooxygenase hydroxylase component, *J. Am. Chem. Soc. 112*, 5861−5865.
24. Liu, Y., Nesheim, J. C., Lee, S.-K., and Lipscomb, J. D. (1995) Gating effects of component B on $O_2$-activation by the methane monooxygenase hydroxylase component, *J. Biol. Chem. 270*, 24662−24665.
25. Wallar, B. J., and Lipscomb, J. D. (2001) Methane monooxygenase component B mutants alter the kinetics of steps throughout the catalytic cycle, *Biochemistry 40*, 2220−2233.
26. Froland, W. A., Andersson, K. K., Lee, S.-K., Liu, Y., and Lipscomb, J. D. (1992) Methane monooxygenase component B and reductase alter the regioselectivity of the hydroxylase component catalyzed reactions: A novel role for protein−protein interactions in oxygenase mechanisms, *J. Biol. Chem. 267*, 17588−17597.
27. Gallagher, S. C., Callaghan, A. J., Zhao, J., Dalton, H., and Trewhella, J. (1999) Global conformational changes control the reactivity of methane monooxygenase, *Biochemistry 38*, 6752−6760.
28. Liu, Y., Nesheim, J. C., Paulsen, K. E., Stankovich, M. T., and Lipscomb, J. D. (1997) Roles of the methane monooxygenase reductase component in the regulation of catalysis, *Biochemistry 36*, 5223−5233.
29. Gassner, G. T., and Lippard, S. J. (1999) Component interactions in the soluble methane monooxygenase system from *Methylococcus capsulatus* (Bath), *Biochemistry 38*, 12768−12785.
30. Blommel, P. G., and Fox, B. G. (2005) Fluorescence anisotropy assay for proteolysis of specifically labeled fusion proteins, *Anal. Biochem. 336*, 75−86.
31. Thao, S., Zhao, Q., Kimball, T., Steffan, E., Newman, C. S., Fox, B. G., and Wrobel, R. L. (2004) Results from high-throughput DNA cloning of *Arabidopsis thaliana* target genes by site-specific recombination, *J. Struct. Funct. Genomics 5*, 267−276.
32. Studts, J. M., Mitchell, K. H., Pikus, J. D., McClay, K., Steffan, R. J., and Fox, B. G. (2000) Optimized expression and purification of toluene 4-monooxygenase hydroxylase, *Protein Expression Purif. 20*, 58−65.
33. Griffin, B. A., Adams, S. R., and Tsien, R. Y. (1998) Specific covalent labeling of recombinant protein molecules inside live cells, *Science 281*, 269−272.
34. Griffin, B. A., Adams, S. R., Jones, J., and Tsien, R. Y. (2000) Fluorescent labeling of recombinant proteins in living cells with FLAsH, *Methods Enzymol. 327*, 565−578.
35. Adams, S. R., Campbell, R. E., Gross, L. A., Martin, B. R., Walkup, G. K., Yao, Y., Llopis, J., and Tsien, R. Y. (2002) New biarsenical ligands and tetracysteine motifs for protein labeling in vitro and in vivo: synthesis and biological applications, *J. Am. Chem. Soc. 124*, 6063−6076.
36. Xia, B., Pikus, J. D., Xia, W., McClay, K., Steffan, R. J., Chae, Y. K., Westler, W. M., Markley, J. L., and Fox, B. G. (1999)

Detection and classification of hyperfine-shifted $^{1}H$, $^{2}H$, and $^{15}N$ resonances of the Rieske ferredoxin component from toluene 4-monooxygenase, *Biochemistry 38*, 727−739.
37. Lountos, G. T., Mitchell, K. H., Studts, J. M., Fox, B. G., and Orville, A. M. (2005) Crystal structures and functional studies of T4moD, the toluene 4-monooxygenase catalytic effector protein, *Biochemistry 44*, 7131−7142.
38. Hunsicker-Wang, L. M., Heine, A., Chen, Y., Luna, E. P., Todaro, T., Zhang, Y. M., Williams, P. A., McRee, D. E., Hirst, J., Stout, C. D., and Fee, J. A. (2003) High-resolution structure of the soluble, respiratory-type Rieske protein from Thermus thermophilus: analysis and comparison, *Biochemistry 42*, 7303−7317.
39. Colbert, C. L., Couture, M. M., Eltis, L. D., and Bolin, J. T. (2000) A cluster exposed: structure of the Rieske ferredoxin from biphenyl dioxygenase and the redox properties of Rieske Fe−S proteins, *Struct. Folding Des. 8*, 1267−1278.
40. Byrne, A. M., Kukor, J. J., and Olsen, R. H. (1995) Sequence analysis of the gene cluster encoding toluene-3-monooxygenase from *Pseudomonas pickettii* PKO1, *Gene 154*, 65−70.
41. Seybold, P. G., Gouterman, M., and Callis, J. (1969) Calorimetric, photometric and lifetime determinations of fluorescence yields of fluorescein dyes, *Photochem. Photobiol. 9*, 229−242.
42. Lakowicz, J. R. (1999) *Principles of Fluorescence Spectroscopy*, 2nd ed., Kluwer Academic/Plenum Publishers, New York.
43. Brandstetter, H., Whittington, D. A., Lippard, S. J., and Frederick, C. A. (1999) Mutational and structural analyses of the regulatory protein B of soluble methane monooxygenase from *Methylococcus capsulatus* (Bath), *Chem. Biol. 6*, 441−449.
44. Wetter, L. R., and Deutsch, H. F. (1951) Immunological studies on egg white proteins IV. Immunochemical and physical studies of lysozyme, *J. Biol. Chem. 192*, 237−242.
45. Canfield, R. E. (1963) The amino acid sequence of egg white lysozyme, *J. Biol. Chem. 238*, 2698−2707.
46. Eubel, H., Heinemeyer, J., Sunderhaus, S., and Braun, H. P. (2004) Respiratory chain supercomplexes in plant mitochondria, *Plant Physiol. Biochem. 42*, 937−942.
47. Harayama, S., Kok, M., and Neidle, E. L. (1992) Functional and evolutionary relationships among diverse oxygenases, *Annu. Rev. Microbiol. 46*, 565−601.
48. Mason, J. R., and Cammack, R. (1992) The electron-transport proteins of hydroxylating bacterial dioxygenases, *Annu. Rev. Microbiol. 46*, 277−305.
49. Lloyd, J. S., Bhambra, A., Murrell, J. C., and Dalton, H. (1997) Inactivation of the regulatory protein B of soluble methane monooxygenase from *Methylococcus capsulatus* (Bath) by proteolysis can be overcome by a Gly to Gln modification, *Eur. J. Biochem. 248*, 72−79.
50. Chang, S.-L., Wallar, B. J., Lipscomb, J. D., and Mayo, K. H. (2001) Residues in *Methylosinus trichosporium* OB3b methane monooxygenase component B involved in molecular interactions with reduced- and oxidized-hydroxylase component: A role for the N-terminus, *Biochemistry 40*, 9539−9551.
51. Haas, J. A., and Fox, B. G. (2002) Fluorescence anisotropy studies of enzyme−substrate complex formation in stearoyl-ACP desaturase, *Biochemistry 41*, 14472−14481.
52. Mueller, J., Lugovskoy, A. A., Wagner, G., and Lippard, S. J. (2002) NMR structure of the [2Fe-2S] ferredoxin domain from soluble methane monooxygenase reductase and interaction with its hydroxylase, *Biochemistry 41*, 42−51.
53. Morales, R., Charon, M.-H., Hudry-Clergeon, G., Peillot, Y., Norager, S., Medina, M., and Frey, M. (1999) Refined X-ray structures of the oxidized, at 1.3 Å, and reduced, at 1.17 Å, [2Fe-2S] ferredoxin from the cyanobacterium Anabaena PCC7119 show redox-linked conformational changes, *Biochemistry 38*, 15764−15773.
54. Cosper, N. J., Eby, D. M., Kounosu, A., Kurosawa, N., Neidle, E. L., Kurtz, D. M., Jr., Iwasaki, T., and Scott, R. A. (2000) Redox-dependent structural changes in archaeal and bacterial Rieske-type [2Fe-2S] clusters, *Protein Sci. 11*, 2969−2973.
55. Groves, J. T. (2003) The bioinorganic chemistry of iron in oxygenases and supramolecular assemblies, *Proc. Natl. Acad. Sci. U.S.A. 100*, 3569−3574.
56. Smits, T. H., Balada, S. B., Witholt, B., and van Beilen, J. B. (2002) Functional analysis of alkane hydroxylases from gram-negative and gram-positive bacteria, *J. Bacteriol. 184*, 1733−1742.

BI0601611